Chemical Vapor Deposition of Aluminum Nanowires on Metal Substrates for Electrical Energy Storage Applications

James Benson,[†] Sofiane Boukhalfa,[†] Alexandre Magasinski,[†] Alexander Kvit,[‡] and Gleb Yushin[†,*]

[†]School of Materials Science and Engineering, Georgia Institute of Technology, Atlanta, Georgia 30332, United States and, [‡]Materials Science Center & Materials Science Department, University of Wisconsin, Madison, Wisconsin 53706, United States

ABSTRACT

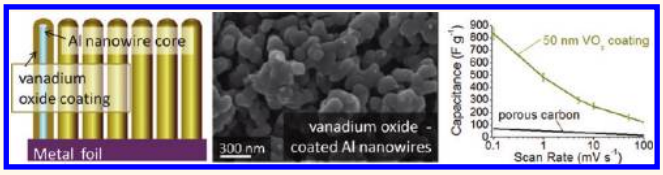

Metal nanowires show promise in a broad range of applications, but many synthesis techniques require complex methodologies. We have developed a method for depositing patterned aluminum nanowires (Al NWs) onto Cu, Ni, and stainless steel substrates using low-pressure decomposition of trimethylamine alane complex. The NWs exhibited an average diameter in the range from 45 to 85 nm, were crystalline, and did not contain a detectable amount of carbon impurities. Atomic layer deposition of 50 nm of vanadium oxide on the surface of Al NW allows fabrication of supercapacitor electrodes with volumetric capacitance in excess of 1400 F·cc^{-3}, which exceeds the capacitance of traditional activated carbon supercapacitor electrodes by more than an order of magnitude.

KEYWORDS: nanowires · chemical vapor deposition · double layer capacitors · supercapacitors · organic electrolytes

Potential use of metal nanowires (NWs) is rapidly growing. Earlier studies of metal NWs were largely motivated by fundamental studies of the effects of constrained dimensions on electrical and thermal conductivities in one-dimensional (1D) conductors[1−3] and magnetic properties of transition metals.[4−6] The size-dependent breakdowns of superconductivity in small diameter NWs draw a particular interest in the past decade.[1−3] Other important potential applications include sensors,[7] ultra-high-density magnetic recording and spintronics,[8] interconnects,[9] transparent current collectors (charge collectors) for touch screens and organic solar cells,[10] catalysis,[11,12] fuel cells,[12] active anodes for Li-ion batteries,[13,14] hydrogen storage,[15] current collectors for Li-ion batteries,[16,17] supercapacitors,[18,19] and capacitors.[20]

Currently, conductive carbon nanotubes (CNTs) mass-produced by chemical vapor deposition (CVD) are explored in some of the discussed above applications. However, the CNT structure suffers from the lack of surface sites available for the formation of chemical bonds with the deposited functional layers (such as metal oxide coatings).[16−20] While surface oxidation of multiwalled CNTs allows for the formation of defects and carboxylic surface groups on their outer walls, the concentration of the functional groups on a CNT surface is significantly smaller than what is available on the metal surfaces. As a result, the quality of a CNT/metal oxide interface is generally inferior to that of a metal/metal oxide one.[21] More importantly, due to the low concentration of free electrons in the CNT, the dc electrical conductivity of the CNT is orders of magnitude smaller than that of Cu, Al, Au, or Ag. Therefore, for most applications requiring high surface area conductors[9,16−20] with low resistance and high concentration of bonding cites on their surface, NWs of low-cost lightweight highly conductive metals (such as Al) may provide superior performance than CNTs.

The most common route for synthesis of metal NWs is electrodeposition.[1−7,16,17] The use of porous alumna templates attached to the conductive substrate surface has become a routine approach for the growth of aligned NWs.[1−3,16,17] The slow deposition rate and the need of tubular templates, however, prevent large-scale commercial synthesis of metal NWs using electrodeposition approaches. Several promising wet chemistry approaches have also been explored for

* Address correspondence to yushin@gatech.edu.

Received for review August 5, 2011 and accepted December 13, 2011.

Published online December 13, 2011
10.1021/nn202979y

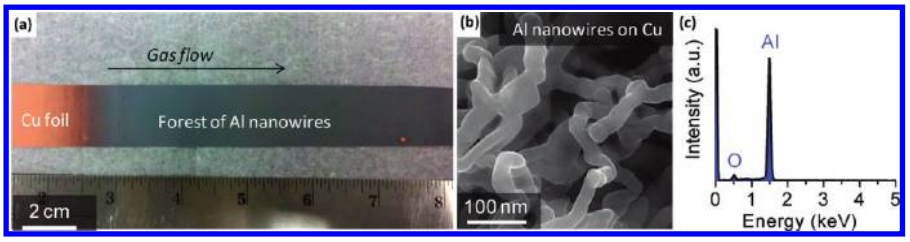

Figure 1. Al NWs grown on a rough Cu foil at 125 °C: (a) optical micrograph showing uniform large-area deposition of Al NWs, (b) SEM micrograph showing a high-resolution image of curved Al NWs produced, and (c) typical EDS spectrum taken at a region containing Al NWs.

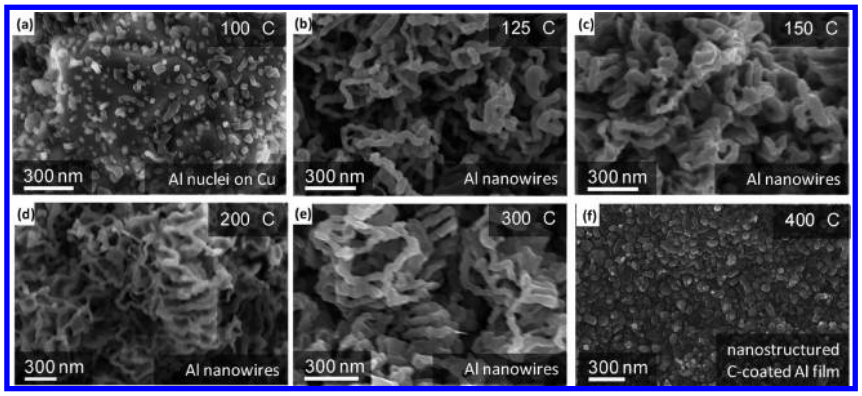

Figure 2. SEM micrographs of CVD deposition of Al NWs onto rough Cu foils at different temperatures: (a) 100 °C, (b) 125 °C, (c) 150 °C, (d) 200 °C, (e) 300 °C, and (e) 400 °C.

metal NW synthesis inside the pores of self-assembled organic nanotubes.[22,23] Yet, the lack of sufficient control over the NW dimensions and limited yield prevented successful commercialization of these synthesis routes. Similar shortcomings are also present in another interesting approach—a glancing angle deposition (GALD), in which a metal is sputtered on a target at a large incident angle.[14] The random initial nuclei formed on the substrate act as seeds for NW growth, while the growth at other areas is restricted by the shadowing of those initially grown nanocrystals.[14]

The rapid growth and large-scale synthesis capability of CVD combined with a high precision in controlling the metal NW dimensions makes CVD one of the most promising approaches for metal NW synthesis. Surprisingly, in contrast to the significant progress achieved in CVD growth of CNTs and semiconductor nanowires, very limited studies report the template-free CVD growth of metal NWs.[24−29] The literature search revealed only reports on CVD growth of Mo NWs on Si, Al_2O_3, and steel;[24] Pt NWs on SiO_2, Ni alloy, and $SrTiO_3$(100);[25] Ni NWs on SiO_2;[28] Cu NWs on SiO_2 and Si;[26,27] and Fe NWs on SiO_2.[29] However, for use of metal NWs in energy storage devices,[13,14,16−20] an abundant, low-cost, highly conductive, corrosion-resistant, and lightweight Al could be of higher demand. Particularly, if Al NWs are grown on conductive metal foil substrates in order to establish a good electrical contact within an electrode. To the best of our knowledge, however, there have been no reports on Al NW growth by CVD on any substrate. Furthermore, we were unable to find reports on the patterned CVD growth of metal NWs, needed for discrete device fabrication.[20]

In this article, we report for the first time a patterned growth of freestanding Al NWs on Ni, Fe, and Cu surfaces using trimethylamine alane (TMAA) as an organometallic CVD precursor. We further demonstrate that the deposition of metal oxides on the Al NW surface allows one to achieve one of the highest specific capacitances reported to date for supercapacitor applictions. In our proof-of-concept studies, we utilized vanadium oxide (VO_x) as a coating material due its chemical stability, wide availability, and the large potential window for oxidation/reduction reactions to occur.[30−37] In order to synthesize the Al NW−VO_x composite electrodes, we employed atomic layer deposition (ALD) to uniformly deposit VO_x onto Al NW substrates. To the best of our knowledge, ALD technique has never been employed for supercapacitor applications and the achieved gravimetric capacitance of up to 887 F/g (based on the mass of Al nanowires and a metal oxide) is higher than the specific capacitance of 601 F/g recently demonstrated in the MnO_2−nanoporous gold nanocomposite.[19] The VO_x-coated Al nanowire electrodes with 30−50% of the pore volume available for electrolyte access show volumetric capacitance of 1390−1950 F/cc, which exceeds the volumetric capacitance of porous carbons and many carbon−metal oxide composites by more than an order of magnitude.[14,38−44]

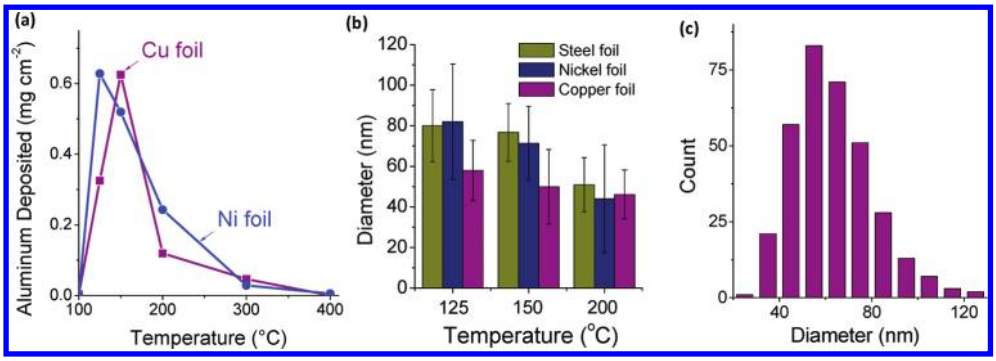

Figure 3. Diameter and deposition rate of Al nanowires on metal foil substrates: (a) mass of Al nanowires deposited on metal foil substrates at different temperatures for 1 h; (b) average diameter of Al nanowires grown on several metal substrates as a function of deposition temperature; (c) diameter distribution of Al nanowires deposited on Cu foil at 125 °C.

RESULTS AND DISCUSSION

The uniform large area (tens of square centimeters) deposition of Al NWs was successfully achieved on Ni, steel, and Cu foils (Figure 1a) at temperatures as low as 125 °C. Most of the produced NWs had smooth surface with no crystalline facets visible, were 20−120 nm in diameter, and had multiple branches, as visible from scanning electron microscopy (SEM) analyses (Figure 1b). The overall morphology of the NWs was highly tortuous with frequent irregular bends (Figure 1b). The length of the straight segments of the NWs rarely exceeded 300 nm. This wormlike structure of the NWs was observed in all experiments, independent of the substrate employed. SEM image analysis revealed a high volume of pores between the NWs (>93%). Energy-dispersive spectroscopy (EDS) studies confirmed the composition of Al NWs and detected a trace amount of oxygen (Figure 1c), likely from the presence of a native oxide on the Al surface. Importantly, no carbon contaminants were detected at temperatures below 150 °C (Figure 1c).

Deposition temperature was found to have a profound effect on the NW growth rate. CVD deposition at 100 °C was very slow with only isolated Al nuclei observed on the metal substrates after 1 h synthesis (Figure 2a). The successful growth of the NWs was achieved on all substrates within the temperature range of 125−300 °C (Figure 2b−e). However, increasing synthesis temperature above 200 °C caused noticeable co-deposition of carbon, likely due to the pyrolysis of the trimethylamine component of TMAA. At the highest synthesis temperature of 400 °C, the amount of the deposited C reached ~50 atom % according to EDS analysis, and the nonporous nanocrystalline film formed instead of NWs (Figure 2f).

The maximum growth rate was commonly observed at temperatures between 100 and 200 °C (Figure 3a). Temperature of 100 °C and below was too low to provide thermal energy sufficient to overcome the energy barrier needed for the rapid nucleation and growth of Al from the vapor phase. Significant decrease in the Al growth kinetics at temperatures above 300 °C (Figure 3a) was hypothesized to be linked to the C co-deposition. The choice of metal substrates was also found to affect the Al NW growth kinetics. For example, the peak in the Al NW growth rate on Cu and Ni foil substrates takes place at slightly different temperatures, at 125 °C for Ni and 150 °C for Cu (Figure 3a). The slight difference is explained by the differences in the energies of the Ni/gas, Ni/Al, Cu/gas, and Cu/Al interfaces, which should affect the nucleation barrier. Additionally, we cannot exclude a possible effect of the H_2 absorption by Ni on the NW nucleation and growth. Hydrogen desorption is known to be the rate-controlling step in TMAA decomposition, and the increased removal of surface H_2 due to its absorption by Ni may similarly explain the increased growth kinetics observed at lower temperatures.[45]

In contrast to our initial expectations rationalized by the higher mobility of surface atoms at elevated temperatures, increasing the synthesis temperature did not increase the average diameter of NWs. In contrast, this temperature increase, in fact, reduced the average diameter of NWs grown on metal substrates (Figure 3b). The observed decrease in the diameter could be related to the smaller size of stable nuclei, expected at higher temperatures where the nucleation barrier is lower. Figure 3c shows a typical NW diameter distribution with an average diameter of 63 nm and a standard deviation of 17 nm, as measured using SEM image analysis. Very similar distributions with average diameters of 45−87 nm and standard deviations of 25% were observed in all substrates and deposition parameters.

The virtually no dependence of the average NW diameter on the length of the deposition process or on the distance from the metal foil substrate suggests that incorporation of Al takes place primarily on the NW tips and not onto the sidewalls of the NWs. This was surprising because no metal catalyst was used and, therefore, one may expect that a sticking coefficient of atoms onto different Al surfaces should not demonstrate very large differences. We propose two possible explanations: either the growth process is self-catalytic or there is a large TMAA concentration gradient at the gas/Al NW forest interface. This concentration gradient may arise if the decomposition of the TMAA on the Al

NW surface is so fast that only a small fraction of the TMAA molecules diffuse into the depth of the Al NW forest. Alternatively, a self-catalytic growth may take place when a freshly formed Al layer on the tip has sufficiently lower energy barrier (in other words, it has a higher surface energy because of the higher nanoscale roughness or higher concentration of defects at the NW tip) than the sidewalls of the NWs. We should additionally note that the NW tips may have higher local temperature because of the heat released upon the exothermic decomposition of TMAA.[45] This higher temperature at the tips may significantly reduce the energy barrier and support the tip-based growth.

The transmission electron microscopy (TEM) studies showed the crystalline structure and dense (no voids) morphology of the NWs (Figure 4a,b). In spite of the tortuous shape of the NWs, TEM studies demonstrated most of the NWs to be free from extended defects. This indicates a stress relaxation (commonly by slipping of extended defects to the NW surface) either during or after the growth. We found only a few mirror-like twin boundaries in Al NWs, commonly in those having larger diameters (Figure 4a,b). Twinning directions are reported in ref 46. Although twinning is an important and quite common mechanism for plastic deformation in metals, pure bulk Al very rarely undergoes twinning due to its very high stacking fault energy (SFE).[42,47] According to Warner *et al.*,[47] twinning during deformations was never observed experimentally in Al and only happened at high strain rates in computer simulations or in nanocrystals that deform under very high stresses at low temperatures.[48,49] Therefore, our observation of twin boundaries in Al NWs, in fact, suggests significant stresses during their synthesis. We postulate that these stresses were caused by the local temperature variations caused by the exothermic nature of the trimethylamine alane precursor surface decomposition process.[50] EDS performed on individual NWs (Figure 4c) showed spectra identical to that of the NW forest (Figure 1c), confirming high purity and uniform oxide content in the produced NWs.

In support of our hypothesis on the negative effect of carbon on the NW nucleation and growth (Figure 2f), we found various carbon and polymer coatings on the metal foils' surface to efficiently prevent formation and growth of Al NWs. Due to the low synthesis temperature and the absence of oxygen in our system (Ar is used as a carrier gas), most polymers remain intact or carbonize during the NW deposition. In contrast to native oxide-coated metal surfaces, polymers' presence prevents formation of the stable Al nuclei, emphasizing the importance of the substrate−Al interactions. Using this simple polymer coating method, we successfully produced a patterned Al NW forest on Cu foils (Figure 5). We expect the patterned growth to be important for some of the future device applications.

X-ray diffraction (XRD) analysis was used to independently investigate the crystallinity of the synthesized

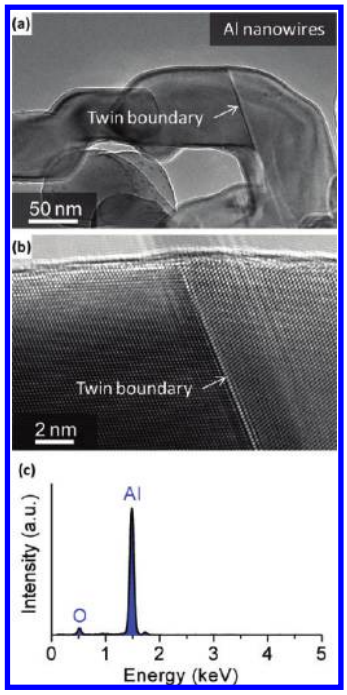

Figure 4. (a) Low- and (b) high-resolution TEM micrographs showing a twin boundary within an Al NW grown on the Cu surface at 125 °C; (c) EDS spectra taken from a single Al NW.

Al NWs on the variety of substrates and to confirm the lack of crystalline aluminum oxide and aluminum carbide impurities (Figure 6). A brief Williamson−Hall analysis estimated the grain size to be in the range of 40−100 nm, which agrees well with the values for the NW diameters observed in SEM and TEM studies (Figures 2−4). This analysis also suggested microstrain of up to 9%. The intensity profile for Al NW diffraction pattern matches that for powder diffraction, as expected from the unaligned nature of the synthesized Al NW forests (Figures 1b and 2b−e).

To evaluate the electrochemical activity of the grown Al NWs, we compared cyclic voltammetry experiments performed on the NWs with that on 17 μm Al foil samples. The experiments were performed within the voltage range of 1 to 0.01 V *vs* Li/Li^+ at a scan rate of 1 mV/s. These results showed an order of magnitude higher Li-ion insertion and extraction current densities for the NW sample than that for the plain Al foil (Figure 7), confirming the significantly higher electrochemically active surface area of Al NWs.

Electrodes produced by the atomic layer deposition (ALD) of vanadium oxide (VO_x) on the surface of Al NWs were evaluated for supercapacitor applications to provide an experimental demonstration or a proof-of-concept for the Al NW application. In our view, the 1D geometry of nanostructured NWs may offer some unique advantages, including higher thermal and electrical conductivity and higher power density of the NW-based energy storage devices.[51] In an ideal case of perfectly straight and aligned NWs (Figure 8a), the pores between them would allow for the shortest ion

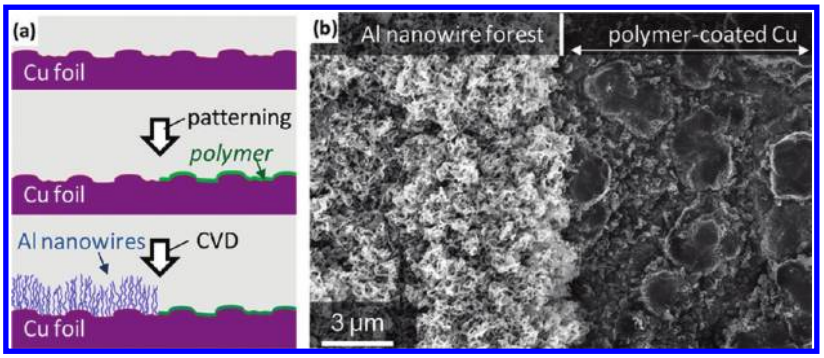

Figure 5. Patterned Al nanowire growth: (a) schematic of the process, (b) SEM micrograph of a patterned Al nanowire growth on a rough Cu foil at 125 °C. In this case, the growth on a portion of the Cu foil was prevented by the deposition of a thin layer of a methylmethacrylate-based polymer.

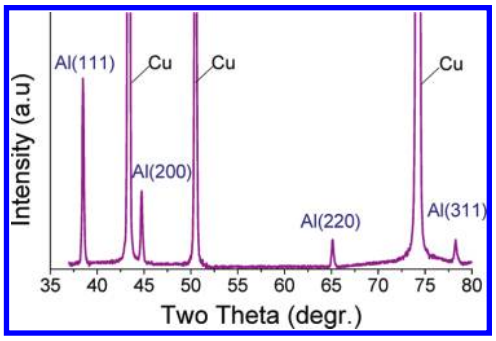

Figure 6. XRD pattern of Al nanowires grown on a rough Cu foil at 125 °C.

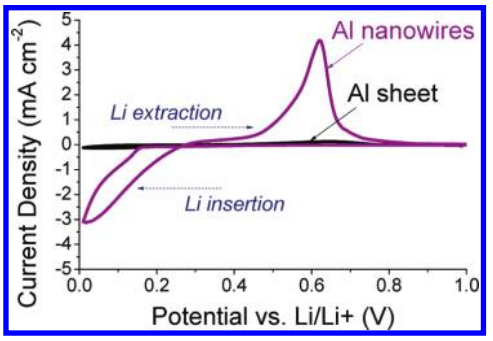

Figure 7. Electrochemical activity of Al nanowires in Li half-cells: cyclic voltammetry recorded at 1 mV/s showing reversible electrochemical interaction of Li^+ ions with Al nanowire electrodes and flat Al sheets.

transport distance within the electrode, thus contributing to minimizing the charging or discharging time. In fact, in our prior studies on pure carbon supercapacitors, we demonstrated that changing the pores within individual porous carbon particles from tortuous to straight can reduce the charging time by 3 orders of magnitude.[39] When nanopores are not straight but relatively large (>2 nm) (Figure 1f), very high rate performance can still be achieved.[41,44]

Both SEM and TEM studies of the VO_x ALD deposited on the surface of the selected Al NW samples showed a high degree of coating uniformity (Figure 8b,c). TEM studies additionally showed the highly disordered nature of the deposited oxide, while SEM analyses detected reduction of the remaining VO_x-coated Al NW electrode porosity to below 50% (Figure 8b). EDS studies, in turn, confirmed the high purity of the deposited VO_x layer (Figure 8d). TEM studies as well as SEM image analysis before and after VO_x depositions were used to estimate the coating thicknesses.

An electrochemically active VO_x offers some of the highest capacitance ever demonstrated in organic electrolytes[30−37] (also Figure 8e) but suffers from very low electrical conductivity. The use of lightweight highly conductive Al NW (Figure 8a) overcomes this key limitation. At a very slow slew rate of 0.01 $mV \cdot s^{-1}$, the specific (gravimetric) capacitance of the 50 nm coating approaches 964 $F \cdot g^{-1}$, but it drops to 836 $F \cdot g^{-1}$ and further to 483 $F \cdot g^{-1}$ at 0.1 and 1 $mV \cdot s^{-1}$, respectively. The obtained values are moderately high as compared to 620−2150 $F \cdot g^{-1}$ reported in aerogels and xerogels when measured with a "sticky carbon" technique needed to overcome their low electrical conductivity during measurements.[34] In spite of the relatively large oxide thickness, gravimetric capacitance advantage over activated carbon used in commercial devices can be maintained even at high sweep rates (Figure 8f) and even when the mass of Al is taken into account. Indeed, assuming a density of 3.3 $g \cdot cc^{-1}$ for VO_x and 2.7 $g \cdot cc^{-1}$ for Al, we can easily calculate that the relative weight of Al in a core−shell NW (Figure 8a) composed of a 45 nm diameter Al core and a 50 nm VO_x shell is only 8 wt %. This is a typical contribution of either a binder or conductive carbon additives in commercial activated carbon-based supercapacitors. The key advantage of the proposed technology over conventionally used porous carbons, however, is significantly higher density and thus volumetric capacitance. Indeed, assuming the true density of the discussed above core−shell NW to be 3.2 $g \cdot cc^{-1}$ and the remaining electrode porosity to be 30−50 vol % (Figure 8b), the volumetric capacity of the NW electrode reaches 1390−1950 $F \cdot cc^{-3}$, which is 10−100 times higher than the volumetric capacitance of various porous carbon electrodes.[14,38−44] This demonstrates the high

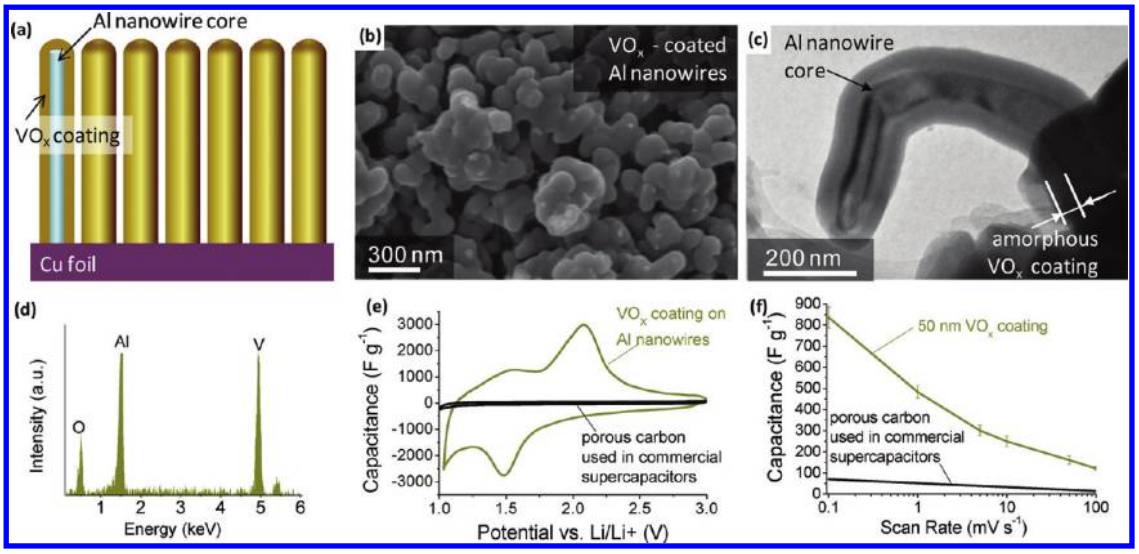

Figure 8. Al nanowire-based supercapacitor: (a) simplified schematic of the electrode; (b) SEM and (c) TEM micrographs of VO_x-coated Al nanowires; (d) EDS spectrum of VO_x-coated Al nanowires; (e) cyclic voltammetry recorded at 0.1 mV/s for VO_x-coated Al nanowire electrode in comparison to that of porous carbon (capacitance is normalized by the active mass); (f) average capacitance as a function of a slew rate for 50 nm VO_x coatings in comparison to that of activated carbon.

potential of the Al NW technology for supercapacitor and other energy storage applications. We expect that if we maintain the same core–shell ratio and decrease the shell thickness while optimizing the VO_x microstructure and electrolyte composition, we will increase both the rate capability and the overall capacitance of the supercapacitor electrodes. Similar techniques of the Al NW growth and ALD oxide deposition could be applicable for the fabrication of electrolytic and regular capacitors as well as electrodes for regular and 3D Li-ion batteries.

CONCLUSIONS

A catalyst-free, low-temperature method of producing high-purity Al NWs on various metal foil substrates using low-pressure CVD technique has been demonstrated. The lack of droplet at the tip suggested a vapor–solid growth mechanism. The presence of twin boundaries in the formed NWs suggested significant plastic deformation during growth. Various factors affecting and explaining the NW growth have been discussed including substrate material and temperature. Thin polymer coatings were found to be highly effective in suppressing the NW growth, thus opening multiple opportunities to produce controlled patterns of Al NWs. The ALD technique experimentally demonstrated the opportunity to form uniform oxide coatings on the NW surface for use in various energy storage devices. Our future studies will be directed toward the size-controlled growth of aligned Al NWs using catalyst-assisted deposition.

EXPERIMENTAL SECTION

Our choice of solid TMAA ($H_3AlN(CH_3)_3$, >95% purity, Gelest, USA) as an Al precursor[52] was motivated by prior studies of CVD deposition of aluminum films for applications in the semiconductor industry, where other organoaluminum precursors, such as trimethylaluminum, triisobutylaluminum, and dimethylaluminum hydride showed tendencies for aluminum carbide contamination.[50,53] For CVD synthesis, we used a low-pressure (2 Torr) hot-walled horizontal quartz tube reactor having 44 mm inner diameter. Ultra-high-purity Ar (99.999%, Air Gas, USA) was used to carry the TMAA vapors to the reaction zone by flowing through a packed bed of TMAA powder at the flow rate of 50 cc/min. The low pressure in the reactor was maintained using a mechanical pump and monitored using a convection gauge. CVD deposition experiments were performed at 100, 125, 150, 200, 300, and 400 °C for 1 h periods. Substrates were prepared of Ni, Cu, and 304 stainless steel foils (Alfa Aesar, USA). In addition, rough Cu foil with the coarse surface produced by electrodepositing Cu on Cu (Fukuda, Japan) was employed to study the effects of surface roughness on Al nanowire deposition rate and morphology. Similarly, the surface chemistry was studied using smooth Cu foils with a 10 nm layer of thermally evaporated ultrahigh purity (99.999%) Fe. The mass of these samples was measured before and after deposition using an analytical balance having 0.01 mg precision.

ALD deposition was done in a custom-built ALD system consisting of a quartz tube heated in a furnace to 200 °C through which precursor vapors were introduced alternatively. Vanadium tri-*n*-propoxide oxide (Gelest, Inc., USA) and 18 MΩ deionized H_2O were used as precursors and were heated to 100 °C during the deposition. High-purity Ar (99.999%, Air Gas, USA) was used as both carrier and purging gas, and the residence and purging periods were 12 and 1 s, respectively, for the H_2O precursor and 2 s each for the vanadium precursor. All of the precursor gas lines were maintained at 100 °C during the deposition process. The pressure of the system was maintained at 4 Torr throughout the deposition by means of a rotary vacuum pump.

X-ray diffraction (XRD) experiments using Cu Kα radiation were performed with a X'Pert PRO Alpha-1 diffractometer (Panalytical, USA) equipped with a monochromator. Scanning electron microscopy (SEM) and energy-dispersive spectroscopy (EDS) measurements of the nanowire morphology, diameter, and composition were performed using a LEO 1550 microscope (LEO Electron Microscopy Group, DE). ImageJ software was employed for the SEM image analysis to determine the

nanowire diameter distributions.[54] Transmission electron microscopy (TEM and STEM) experiments were done on a FEI Titan 80-300 microscope with a field emission gun equipped with a CEOS probe-side aberration corrector, HAADF detectors, Gatan Tridiem system, and an energy-dispersive X-ray (EDX) system. Point-to-point resolution of this microscope is 2.45 Å in TEM mode and 0.8 Å in STEM mode. All TEM experiments were done at 200 kV.

For electrochemical testing, the working electrodes were spot-welded to 2016 coin cells and assembled in an Ar drybox (<2 ppm H_2O) using a 2325 Celgard (Celgard, USA) separator. The counter and reference electrode was 0.75 mm thick battery grade metallic Li (Alfa Aesar, USA). We selected 1 M $LiPF_6$ salt solution in dimethyl, diethyl, and ethylene carbonate solvents 1:1:1 by volume (Novolyte Technologies, USA) as an electrolyte. Electrodes of 17 μm Al foil were cleaned by acetone and ethanol before assembly, while Al NW and VO_x-coated Al NW electrodes were used as produced. Commercial carbon electrodes were produced using 90 wt % activated carbon (Sanwa Components, USA) and 10 wt % PVDF binder (Kureha, Japan). Cyclic voltammetry was performed using a Solartron 1480A (Solartron Analytical, UK) with the potential being swept from the open circuit potential (OCV) to 0.01 V *vs* Li at a scan rate of 1−0.01 mV/s. Capacitance measurements were performed on as-produced VO_x-coated Al NW using cyclic voltammetry with the potential being swept from 3 to 1 V *vs* Li at a scan rate of 100−0.01 mV/s.

Acknowledgment. This work was partially supported by AFOSR grants FA9550-09-1-0176 and FA9550-09-1-0176 and NSF Grant 0954925.

REFERENCES AND NOTES

1. Zgirski, M.; Riikonen, K. P.; Touboltsev, V.; Arutyunov, K. Size Dependent Breakdown of Superconductivity in Ultranarrow Nanowires. *Nano Lett.* **2005**, *5*, 1029–1033.
2. Zgirski, M.; Riikonen, K. P.; Touboltsev, V.; Arutyunov, K. Y. Quantum Fluctuations in Ultranarrow Superconducting Aluminum Nanowires. *Phys. Rev. B* **2008**, *77*, 054508.
3. Ozer, M. M.; Thompson, J. R.; Weitering, H. H. Hard Superconductivity of a Soft Metal in the Quantum Regime. *Nat. Phys.* **2006**, *2*, 173–176.
4. Guo, Y. G.; Wan, L. J.; Zhu, C. F.; Yang, D. L.; Chen, D. M.; Bai, C. L. Ordered Ni−Cu Nanowire Array with Enhanced Coercivity. *Chem. Mater.* **2003**, *15*, 664–667.
5. Bao, J. C.; Tie, C. Y.; Xu, Z.; Zhou, Q. F.; Shen, D.; Ma, Q. Template Synthesis of an Array of Nickel Nanotubules and Its Magnetic Behavior. *Adv. Mater.* **2001**, *13*, 1631–1633.
6. Ferre, R.; Ounadjela, K.; George, J. M.; Piraux, L.; Dubois, S. Magnetization Processes in Nickel and Cobalt Electrodeposited Nanowires. *Phys. Rev. B* **1997**, *56*, 14066–14075.
7. McGary, P. D.; Tan, L. W.; Zou, J.; Stadler, B. J. H.; Downey, P. R.; Flatau, A. B. Magnetic Nanowires for Acoustic Sensors (Invited). *J. Appl. Phys.* **2006**, *99*, 8B310.
8. Sellmyer, D. J.; Zheng, M.; Skomski, R. Magnetism of Fe, Co and Ni Nanowires in Self-Assembled Arrays. *J. Phys.: Condens. Matter* **2001**, *13*, R433–R460.
9. Kim, T. H.; Zhang, X. G.; Nicholson, D. M.; Evans, B. M.; Kulkarni, N. S.; Radhakrishnan, B.; Kenik, E. A.; Li, A. P. Large Discrete Resistance Jump at Grain Boundary in Copper Nanowire. *Nano Lett.* **2010**, *10*, 3096–3100.
10. Granqvist, C. G. Transparent Conductors as Solar Energy Materials: A Panoramic Review. *Sol. Energy Mater. Sol. Cells* **2007**, *91*, 1529–1598.
11. Huber, G. W.; Shabaker, J. W.; Dumesic, J. A. Raney Ni−Sn Catalyst for H-2 Production from Biomass-Derived Hydrocarbons. *Science* **2003**, *300*, 2075–2077.
12. Lee, E. P.; Peng, Z. M.; Cate, D. M.; Yang, H.; Campbell, C. T.; Xia, Y. Growing Pt Nanowires as a Densely Packed Array on Metal Gauze. *J. Am. Chem. Soc.* **2007**, *129*, 10634–10635.
13. Hamon, Y.; Brousse, T.; Jousse, F.; Topart, P.; Buvat, P.; Schleich, D. M. Aluminum Negative Electrode in Lithium Ion Batteries. *J. Power Sources* **2001**, *97*−*98*, 185–187.
14. Au, M.; McWhorter, S.; Ajo, H.; Adams, T.; Zhao, Y. P.; Gibbs, J. Free Standing Aluminum Nanostructures as Anodes for Li-Ion Rechargeable Batteries. *J. Power Sources* **2010**, *195*, 3333–3337.
15. Sakintuna, B.; Lamari-Darkrim, F.; Hirscher, M. Metal Hydride Materials for Solid Hydrogen Storage: A Review. *Int. J. Hydrogen Energy* **2007**, *32*, 1121–1140.
16. Shaijumon, M. M.; Perre, E.; Daffos, B.; Taberna, P. L.; Tarascon, J. M.; Simon, P. Nanoarchitectured 3D Cathodes for Li-Ion Microbatteries. *Adv. Mater.* **2010**, *22*, 4978–4981.
17. Taberna, L.; Mitra, S.; Poizot, P.; Simon, P.; Tarascon, J. M. High Rate Capabilities Fe_3O_4-Based Cu Nano-Architectured Electrodes for Lithium-Ion Battery Applications. *Nat. Mater.* **2006**, *5*, 567–573.
18. Portet, C.; Taberna, P. L.; Simon, P.; Laberty-Robert, C. Modification of Al Current Collector Surface by Sol−Gel Deposit for Carbon-Carbon Supercapacitor Applications. *Electrochim. Acta* **2004**, *49*, 905–912.
19. Lang, X.; Hirata, A.; Fujita, T.; Chen, M. Nanoporous Metal/Oxide Hybrid Electrodes for Electrochemical Supercapacitors. *Nat. Nanotechnol.* **2011**in press.
20. Banerjee, P.; Perez, I.; Henn-Lecordier, L.; Lee, S. B.; Rubloff, G. W. Nanotubular Metal−Insulator−Metal Capacitor Arrays for Energy Storage. *Nat. Nanotechnol.* **2009**, *4*, 292–296.
21. Centi, G.; Gangeri, M.; Fiorello, M.; Perathoner, S.; Amadou, J.; Begin, D.; Ledoux, M. J.; Pham-Huu, C.; Schuster, M. E.; Su, D. S.; Tessonnier, J. P.; Schlogi, R. The Role of Mechanically Induced Defects in Carbon Nanotubes to Modify the Properties of Electrodes for Pem Fuel Cell. *Catal. Today* **2009**, *147*, 287–299.
22. Reches, M.; Gazit, E. Casting Metal Nanowires within Discrete Self-Assembled Peptide Nanotubes. *Science* **2003**, *300*, 625–627.
23. Hong, B. H.; Bae, S. C.; Lee, C. W.; Jeong, S.; Kim, K. S. Ultrathin Single-Crystalline Silver Nanowire Arrays Formed in an Ambient Solution Phase. *Science* **2001**, *294*, 348–351.
24. Zhou, J.; Deng, S. Z.; Gong, L.; Ding, Y.; Chen, J.; Huang, J. X.; Xu, N. S.; Wang, Z. L. Growth of Large-Area Aligned Molybdenum Nanowires by High Temperature Chemical Vapor Deposition: Synthesis, Growth Mechanism, and Device Application. *J. Phys. Chem. B* **2006**, *110*, 10296–10302.
25. Lo Nigro, R.; Malandrino, G.; Fiorenza, P.; Fragala, I. L. Template-Free and Seedless Growth of Pt Nanocolumns: Imaging and Probing Their Nanoelectrical Properties. *ACS Nano* **2007**, *1*, 183–190.
26. Kim, C.; Gu, W. H.; Briceno, M.; Robertson, I. M.; Choi, H.; Kim, K. Copper Nanowires with a Five-Twinned Structure Grown by Chemical Vapor Deposition. *Adv. Mater.* **2008**, *20*, 1859–1863.
27. Choi, H.; Park, S. H. Seedless Growth of Free-Standing Copper Nanowires by Chemical Vapor Deposition. *J. Am. Chem. Soc.* **2004**, *126*, 6248–6249.
28. Chan, K. T.; Kan, J. J.; Doran, C.; Lu, O. Y.; Smith, D. J.; Fullerton, E. E. Oriented Growth of Single-Crystal Ni Nanowires onto Amorphous SiO_2. *Nano Lett.* **2010**, *10*, 5070–5075.
29. Bien, D. C. S.; Bain, M. F.; Low, Y. H.; Mitchell, N. S. J.; Armstrong, M. B.; Gamble, H. S. Multiple Self-Aligned Iron Nanowires by a Dual Selective Chemical Vapor Deposition Process. *Electrochem. Solid-State Lett.* **2007**, *10*, H251–H253.
30. Sun, D.; Kwon, C. W.; Baure, G.; Richman, E.; MacLean, J.; Dunn, B.; Tolbert, S. H. The Relationship between Nanoscale Structure and Electrochemical Properties of Vanadium Oxide Nanorolls. *Adv. Funct. Mater.* **2004**, *14*, 1197–1204.
31. Sudant, G.; Baudrin, E.; Dunn, B.; Tarascon, J. M. Synthesis and Electrochemical Properties of Vanadium Oxide Aerogels Prepared by a Freeze-Drying Process. *J. Electrochem. Soc.* **2004**, *151*, A666–A671.
32. Sakamoto, J. S.; Dunn, B. Vanadium Oxide−Carbon Nanotube Composite Electrodes for Use in Secondary Lithium Batteries. *J. Electrochem. Soc.* **2002**, *149*, A26–A30.
33. Rolison, D. R.; Dunn, B. Electrically Conductive Oxide Aerogels: New Materials in Electrochemistry. *J. Mater. Chem.* **2001**, *11*, 963–980.

34. Dong, W.; Rolison, D. R.; Dunn, B. Electrochemical Properties of High Surface Area Vanadium Oxide Aerogels. *Electrochem. Solid-State Lett.* **2000**, *3*, 457–459.
35. Shembel, E.; Apostolova, R.; Nagirny, V.; Aurbach, D.; Markovsky, B. Synthesis, Investigation and Practical Application in Lithium Batteries of Some Compounds Based on Vanadium Oxides. *J. Power Sources* **1999**, *80*, 90–97.
36. Chen, Z.; Augustyn, V.; Wen, J.; Zhang, Y. W.; Shen, M. Q.; Dunn, B.; Lu, Y. F. High-Performance Supercapacitors Based on Intertwined CNT/V_2O_5 Nanowire Nanocomposites. *Adv. Mater.* **2011**, *23*, 791–795.
37. Dong, W.; Sakamoto, J.; Dunn, B. Electrochemical Properties of Vanadium Oxide Aerogels and Aerogel Nanocomposites. *J. Sol–Gel Sci. Technol.* **2003**, *26*, 641–644.
38. Korenblit, Y.; Rose, M.; Kockrick, E.; Borchardt, L.; Kvit, A.; Kaskel, S.; Yushin, G. High-Rate Electrochemical Capacitors Based on Ordered Mesoporous Silicon Carbide-Derived Carbon. *ACS Nano* **2010**, *4*, 1337–1344.
39. Kajdos, A.; Kvit, A.; Jones, F.; Jagiello, J.; Yushin, G. Tailoring the Pore Alignment for Rapid Ion Transport in Microporous Carbons. *J. Am. Chem. Soc.* **2010**, *132*, 3252.
40. Chmiola, J.; Largeot, C.; Taberna, P. L.; Simon, P.; Gogotsi, Y. Monolithic Carbide-Derived Carbon Films for Micro-Supercapacitors. *Science* **2010**, *328*, 480–483.
41. Pech, D.; Brunet, M.; Durou, H.; Huang, P. H.; Mochalin, V.; Gogotsi, Y.; Taberna, P. L.; Simon, P. Ultrahigh-Power Micrometre-Sized Supercapacitors Based on Onion-like Carbon. *Nat. Nanotechnol.* **2010**, *5*, 651–654.
42. Al-Samman, T. Comparative Study of the Deformation Behavior of Hexagonal Magnesium-Lithium Alloys and a Conventional Magnesium AZ31 Alloy. *Acta Mater.* **2009**, *57*, 2229–2242.
43. Hulicova-Jurcakova, D.; Seredych, M.; Lu, G. Q.; Bandosz, T. J. Combined Effect of Nitrogen- and Oxygen-Containing Functional Groups of Microporous Activated Carbon on Its Electrochemical Performance in Supercapacitors. *Adv. Funct. Mater.* **2009**, *19*, 438–447.
44. Portet, C.; Yushin, G.; Gogotsi, Y. Electrochemical Performance of Carbon Onions, Nanodiamonds, Carbon Black and Multiwalled Nanotubes in Electrical Double Layer Capacitors. *Carbon* **2007**, *45*, 2511–2518.
45. Dubois, L. H.; Zegarski, B. R.; Gross, M. E.; Nuzzo, R. G. Aluminum Thin Film Growth by the Thermal Decomposition of Triethylamine Alane. *Surf. Sci.* **1991**, *244*, 89–95.
46. Boo, J.-H.; Lee, S.-B.; Yu, K.-S.; Koh, W.; Kim, Y. Growth of Magnesium Oxide Thin Films Using Single Molecular Precursors by Metal–Organic Chemical Vapor Deposition. *Thin Solid Films* **1999**, *341*, 63–67.
47. Warner, D. H.; Curtin, W. A.; Qu, S. Rate Dependence of Crack-Tip Processes Predicts Twinning Trends in F.C.C. Metals. *Nat. Mater.* **2007**, *6*, 876–881.
48. Chen, M. W.; Ma, E.; Hemker, K. J.; Sheng, H. W.; Wang, Y. M.; Cheng, X. M. Deformation Twinning in Nanocrystalline Aluminum. *Science* **2003**, *300*, 1275–1277.
49. Liao, X. Z.; Zhou, F.; Lavernia, E. J.; He, D. W.; Zhu, Y. T. Deformation Twins in Nanocrystalline Al. *Appl. Phys. Lett.* **2003**, *83*, 5062–5064.
50. Carlsson, J.-O.; Jansson, U. Progress in Chemical Vapor Deposition. *Prog. Solid State Chem.* **1993**, *22*, 237–292.
51. Evanoff, K.; Khan, J.; Balandin, A. A.; Magasinski, A.; Ready, W. J.; Fuller, T. F.; Yushin, G. Toward Ultra-Thick Battery Electrodes: Aligned Carbon Nanotube-Enabled Architecture. *Adv. Mater.* **2011**in press.
52. Beach, D. B.; Blum, S. E.; LeGoues, F. K. Chemical Vapor Deposition of Aluminum from Trimethylamine-Alane. *J. Vac. Sci. Technol., A* **1989**, *7*, 3117–3118.
53. Hinnen, C.; Imbert, D.; Siffre, J. M.; Marcus, P. An *In Situ* XPS Study of Sputter-Deposited Aluminium Thin Films on Graphite. *Appl. Surf. Sci.* **1994**, *78*, 219–231.
54. Abramoff, M. D.; Magelhaes, P. J.; Ram, S. J. Image Processing with Imagej. *Biophotonics Int.* **2004**, *11*, 36–42.